Cellulose (2016) 23:493–503
DOI 10.1007/s10570-015-0840-7

ORIGINAL PAPER

A comparison of cellulose nanofibrils produced from *Cladophora glomerata* algae and bleached eucalyptus pulp

Zhouyang Xiang · Wenhua Gao · Liheng Chen · Wu Lan · J. Y. Zhu · Troy Runge

Received: 7 October 2015 / Accepted: 8 December 2015 / Published online: 22 December 2015

Abstract *Cladophora*, a fresh-water green macroalgae, has unique cellulose properties and thus may be promising for production of cellulose nanofibrils (CNFs). Cellulose was extracted from *Cladophora glomerata* and subjected to microfluidization with or without enzymatic hydrolysis pretreatment to produce CNFs. Increasing microfluidization passes produced smaller algal CNFs with more uniform sizes and lower crystallinity. Combining microfluidization with an enzymatic hydrolysis pretreatment, the algal CNFs' crystallinity decreased further, but the diameter distribution showed little change. The algal CNFs were compared to CNFs produced from bleached eucalyptus pulp (BEP), with the algal CNFs having significantly higher crystallinity, smaller diameter and better thermal stability. The XRD spectra of algal and BEP CNFs were simulated by Mercury 3.0 software. The results indicated that BEP CNFs are mainly cellulose Iβ with a random orientation, while algal CNFs are likely a hybrid of cellulose Iα with preferred orientations along the [100] and [010] axes with a March–Dollase factor of 0.65.

Keywords Bleached eucalyptus pulp · Cellulose nanofibrils · *Cladophora glomerata* · Enzymatic hydrolysis · Green algae · X-ray diffraction

Abbreviations

BEP	Bleached eucalyptus pulp
CI	Crystallinity index
CNFs	Cellulose nanofibrils
alg-CNF-10 and alg-CNF-20	Algal CNFs produced by microfluidization only with 10 or 20 passes
alg-CNF-enzy and BEP-CNF-enzy	Algal CNFs or BEP CNFs produced by enzymatic hydrolysis and microfluidization with 20 passes
FWHM	Full width at half maximum

Introduction

Cellulose has been one of the most accessible and widely used bio-materials from ancient times in the forms of wood, paper and cloth. Cellulose polymers

Z. Xiang · W. Gao (✉) · L. Chen
State Key Laboratory of Pulp and Paper Engineering, South China University of Technology, Guangzhou 510640, China
e-mail: segaowenhua@scut.edu.cn

L. Chen · J. Y. Zhu
Forest Products Laboratory, USDA Forest Service, Madison, WI 53726, USA

W. Lan · J. Y. Zhu · T. Runge (✉)
Department of Biological Systems Engineering, University of Wisconsin-Madison, Madison, WI 53706, USA
e-mail: trunge@wisc.edu

are homogeneous and composed exclusively of β-(1 → 4) linked β-D-glucopyranose with degrees of polymerization in the thousands (Moon et al. 2011). The linearity and abundant hydroxyl groups of cellulose molecules facilitate its aggregation into very compact structures due to hydrogen bonds and hydrophobic interactions (Iwamoto et al. 2007). These elementary microfibrils have some degree of crystallinity. The elementary microfibrils further aggregate into nanofibrils and macrofibrils (Hult et al. 2001; Paakko et al. 2007). The macroscopic mechanical strength of cellulose-based materials (i.e. wood) is due to linearity, homogeneity, high degree of polymerization and high crystallinity of cellulose molecules. The cellulose elementary microfibrils have widths of about 5 nm with a very high aspect ratio (Hult et al. 2001; Paakko et al. 2007). The separation of cellulose fiber into nano-scale elementary microfibrils or nanofibrils is of great interest due to their unique optical, rheological and mechanical properties (Paakko et al. 2007; Zhu et al. 2011; Hua et al. 2014). Uniformly separating cellulose fibers into cellulose nanofibrils (CNFs), with their large aspect ratios is difficult. CNFs typically have widths in the 5–40 nm range with lengths of several micrometre (Henriksson et al. 2007; Paakko et al. 2007; Siro and Plackett 2010; Wang et al. 2012).

CNFs are mainly produced from wood or wood pulps (Qing et al. 2013; Wang et al. 2012; Wang and Zhu 2015). CNFs have also been produced using herbaceous lignocelluloses (Alemdar and Sain 2008; Reddy and Yang 2005). Most CNF production processes are expensive due to the difficulties in separating CNFs from the hierarchical lignocellulosic biomass cell structure (Zhu et al. 2011). *Cladophora* and other green algae are highly unexploited bioresources (Hua et al. 2014; Mihranyan 2011). Eutrophication due to agriculture runoff is causing high levels of *Cladophora* green algae in the fresh water system such as the Great Lakes in the United States (Auer et al. 2010). Finding useful applications for this material could encourage harvesting of this abundant material. Inspecting its chemical constituents, *Cladophora* algae contain abundant cellulose (20–30 %), protein and lipid (Mihranyan 2011) suggesting several valorization opportunities in biorefinery systems.

Algal cellulose elementary microfibrils are typically 10–30 nm in width, larger than those in lignocellulosic materials (~5 nm; Mihranyan 2011). Additionally, algal cellulose has unique properties leading to potential applications for drug delivery and fiber/polymer composites Compared with cellulose in lignocelluloses, cellulose in *Cladophora* has a very high degree of crystallinity, that impart inertness to chemical reactions. It also maintains a high specific surface area upon drying, without great hornification or agglomeration, ensuring an excellent redispersibility (Hua et al. 2014; Mihranyan 2011; Strømme et al. 2002). The extraction of algal cellulose usually includes acid hydrolysis and mechanical grinding (Mihranyan et al. 2004; Moon et al. 2011). Nanofibrils of 20–30 nm in width intertwined with each other into a sponge-like structure may be seen from SEM pictures of extracted *Cladophora* cellulose (Mihranyan et al. 2004; Mihranyan 2011). However, regular grinding or milling will not give the algal cellulose nanofibrils a uniform size distribution. Furthermore, although high crystallinity imparts algal cellulose with physical and chemical robustness, it can prevent efficient chemical modifications for alternate properties. Consequently, an effective treatment is needed for producing well-separated nanofibrils with a proper crystallinity from algal cellulose. Here, we use an enzymatic treatment together with an intensive mechanical microfluidization for CNF productions from green algae. The CNFs from green algae were compared with the CNFs from pulp to evaluate their differences using the same method under the similar conditions.

Materials and methods

Materials

Cladophora glomerata (*C. glomerata*) samples were collected from Lake Mendota, Madison, WI in June 2014. Contamination from dirt, plants, and insects was carefully removed through washing and the clean material allowed to air dry. Bleached eucalyptus pulp (BEP) was obtained from a commercial source (Aracruz Cellulose, Brazil). The previously determined chemical composition of this pulp was 78.1 % glucan, 15.3 % xylan and 0.7 % Klason lignin (Wang et al. 2012). Cellulases (Cellic CTec2) with an activity of approximately 150 FPU/mL were provided by Novozymes North America (Franklinton, NC, USA). All other chemicals used in this study were of ACS reagent grade.

Algal cellulose extraction

The algal cellulose extraction process generally followed the procedure described by Mihranyan et al. (2004). Approximately 1 g of clean *C. glomerata* algae sample was bleached with 0.4 g $NaClO_2$ in 10 mL sodium acetate buffer (pH 4.8) at 60 °C for 3 h. The solid fraction was separated and washed until neutrality (pH ~ 7) using a centrifuge (5810R, Eppendorf, Hauppauge, NY, USA). The solids was then mixed with 12.0 mL of 0.5 M NaOH solution and maintained at 60 °C overnight. The resultant material was separated, washed with DI water until supernatant neutrality was achieved, and freeze-dried. After drying, 0.25 g of the material and 6 mL of 5 % HCl were mixed and heated until boiling. After boiling, the mixture was allowed to stand overnight at room temperature. The cellulose was then separated, washed with DI water until supernatant neutrality was achieved, and freeze-dried.

Enzymatic hydrolysis

Enzymatic hydrolysis pretreatments of the algal cellulose and BEP were carried out at solids consistency of 2 % (w/v) in a sodium acetate buffer of pH 4.8. Enzyme charge of 3 FPU/g glucan was used. The slurry was incubated at 50 °C in an incubator shaker (Excella E24, New Brunswick Scientific, Edison, NJ, USA) at 150 rpm for 1, 3, 6, 12, 24, 30 and 48 h. The solids yields of enzymatic hydrolysis were obtained by calculating the weight ratios of enzymatic hydrolysis residues and starting solid substrates.

Mechanical nanofibrillation

BEP and algal cellulose samples (enzymatically treated for 48 h or not treated) were soaked in water overnight and disintegrated in a domestic blender (Waring 700 s) at 20,000 rpm for 30 s to make a 2 wt% suspension. The suspension was diluted to 0.2 wt% and passed through a microfluidizer (M-110EH, Newton, MA, USA) 10 or 20 passes with a 200 μm chamber and 10 or 20 additional passes with an 87 μm chamber.

Characterization methods

Fourier transform infrared (FT-IR) spectra were obtained on a Spectrum 100 FT-IR spectrometer (PerkinElmer, Waltham, MA, USA) equipped with a universal ATR sampling accessory. The spectra were recorded at 25 °C in the range of 650–4000 cm^{-1} for 10 scans.

Cellulose fiber and nanofibril surface morphologies were evaluated using a field emission scanning electron microscope (FE-SEM) (Merlin, Carl Zeiss, Germany) and an atomic force microscope (AFM) (Multimode 8, Bruker, Germany). The diameter distributions of CNFs were obtained by analyzing the SEM pictures through Image-Pro Plus software (Media Cybernetics, Silver Spring, USA); the distribution analyses were achieved after measuring at least 130 individual nanofibrils or sections (Wang et al. 2012).

Dynamic thermogravimetric analysis (TGA) was performed on a thermogravimetric analyzer (Q500, TA Instruments, New Castle, DE). The system was operated in a temperature range from 30 to 700 °C with a heating rate of 10 °C/min and supplied with high purity nitrogen at a flow rate of 50 mL/min.

X-ray diffraction (XRD) measurements were performed by a Rigaku D/Max-III X-ray diffraction analyzer. The samples were prepared as loose powders. The diffracted intensity of CuKα radiation ($\lambda = 1.54056$ Å) at 40 kV and 40 mA was measured in a 2θ range of 4°–50°. The Segal crystallinity index (CI) was calculated by using the following equation (Segal et al. 1959):

$$\mathrm{CI} = \frac{(I_{\max} - I_{\min})}{I_{\min}} \times 100\,\%$$

where $I_{\max}$ is the intensity of the highest peak, and $I_{\min}$ is the minimum intensity at a 2θ angle close to 18° for cellulose I.

Diffraction patterns were simulated by using the crystal information files (cif) containing the published coordinates of the asymmetric units of cellulose Iα and cellulose Iβ from the studies of Nishiyama et al. (2002, 2003) and the Mercury 3.0 program (French 2014; Macrae et al. 2008). This program calculated a diffraction pattern of completely periodic crystals of various sizes, which were determined by the input full width at half maximum (FWHM). The CuKα wavelength was set at 1.54056 Å. Random orientations or preferred orientation with March–Dollase factors were used.

Crystallite width perpendicular to the (110) plane for cellulose Iα and the (200) plane for cellulose Iβ,

and crystallite length perpendicular to the (004) plane were calculated by the Scherrer equation (Leppänen et al. 2009; Yue et al. 2015).

$$\tau = \frac{K\lambda}{\beta \cos\theta}$$

where τ is the crystallite width or length in Å, K is the shape correction factor (1.0), λ is the radiation wavelength (1.54056 Å), β is the FWHM of the highest diffraction peak in radians, and θ is the half 2θ angle of the peaks for (110), (200), or (004) planes.

Results and discussion

Characterization of algal cellulose

The yield of the extracted *C. glomerata* cellulose was 21.6 %, which is consistent with previous studies that green algae have cellulose content of 20–30 % (Mihranyan 2011). The FTIR spectrum was acquired (Fig. 1). The broad peak at 3340 cm^{-1} mainly corresponds to O–H stretching of the CH_2–OH structure on cellulose (Moran et al. 2008). The peaks at 2900 and 1372 cm^{-1} were due to the C–H vibration and bending, respectively; the peaks at 1170 and 1108 cm^{-1} correspond to the glycosidic bonds (C–O–C) and C–OH, respectively; the peak at 1060 cm^{-1} is due to C–C stretching (Moran et al. 2008; Mwaikambo and Ansell 2002). Peaks in the range of 1500–1660 cm^{-1} would indicate proteins; their absence indicates that the extracted *C. glomerata* cellulose contains only an undetectable amount of proteins and has high purity (Jagadeesh et al. 2011).

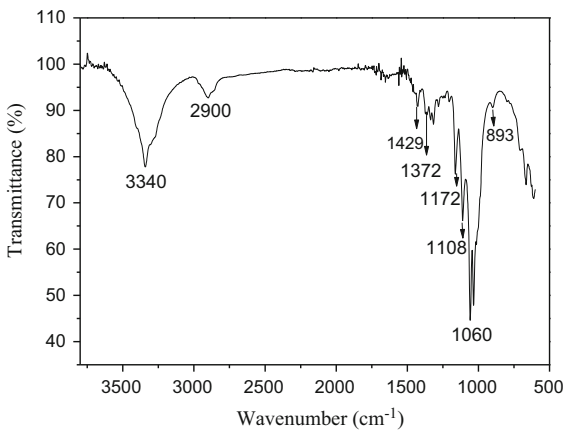

Fig. 1 FTIR spectrum of extracted *C. glomerata* cellulose

Nelson and O'Connor (1964) found that the infrared ratio of FTIR peaks at 1372 and 2900 cm^{-1} (H_{1372}/H_{2900}) reflects the cellulose crystallinity. According to H_{1372}/H_{2900} (0.965) in the FTIR spectrum (Fig. 1), the crystallinity of *C. glomerata* cellulose can be estimated as 96.5 %, which agrees with the 92.2 % Segal crystallinity index (CI) obtained from the XRD measurement (Fig. 2a). The crystallinity of the extracted *C. glomerata* cellulose is consistent with previous studies. Camacho et al. (2013) studied *Cladophora* algae from the lakes in the Philippines and estimated the cellulose crystallinity by FTIR to be 95 %. Mihranyan et al. (2004) studied *Cladophora* sp. algae harvested from the Baltic Sea and found that the cellulose crystallinity was 95.2 %.

The morphology of the *C. glomerata* cellulose is demonstrated in the SEM pictures (Fig. 3a, b). From the picture of low magnification (Fig. 3a), bundles of *C. glomerata* cellulose fiber can be seen. Each fiber has a diameter of 30–80 μm, and as can be seen from the pictures with higher magnifications (Fig. 3b), is composed of nanofibrils 10–40 nm in width. The threadlike nanofibrils intertwined with each other forming a sponge-like or web-like structure, which is consistent with previous studies of *Cladophora* algal cellulose structure (Mihranyan et al. 2004; Mihranyan 2011).

Mechanical nanofibrillation of algal cellulose without enzymatic treatment

A microfluidizer was used to disintegrate *C. glomerata* cellulose into nanofibrils. During microfluidization, fibers are first run through an intensifier pump and the pressure is increased to 275 MPa (40,000 psi); the fibers are then passed through an interaction chamber with micro-channels and defibrillated by high shear forces and impacts against the channel wall (Spence et al. 2011). In this study, the algal cellulose was passed through the microfluidizer 10 or 20 passes using a 200 μm chamber and 10 or 20 additional passes using an 87 μm chamber. The resulting CNFs were labeled as alg-CNF-10 and alg-CNF-20, respectively.

The Segal CI of the algal CNFs was calculated through XRD measurements. Microfluidization reduced the crystallinity of algal cellulose (Fig. 2a),

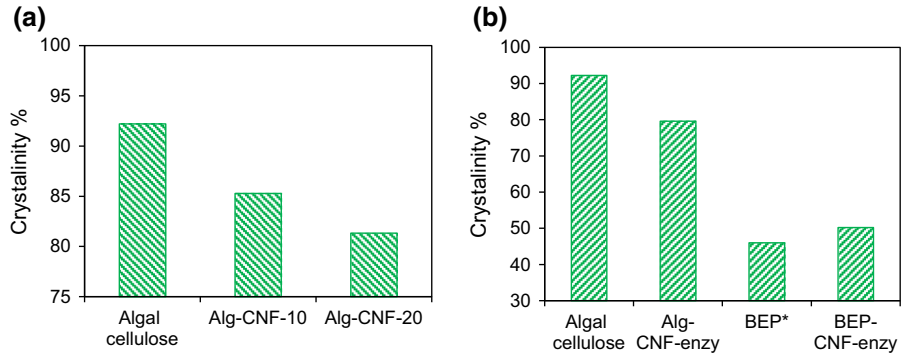

Fig. 2 Segal crystallinity index [*BEP data from Qing et al. (2013)]

and more passes in microfluidization resulted in a lower crystallinity. It is known that mechanical processing of cellulose can cause damage to crystals, resulting in reduced crystallinity (Wang et al. 2012; Iwamoto et al. 2007). The Segal CI of alg-CNF-10 and alg-CNF-20 decreased to 85.3 and 81.3 %, respectively, from 92.2 % of the algal cellulose without microfluidization; i.e. the reduction in CI was 6.9 % units with ten passes in the 200 μm chamber, and additional ten passes in the same chamber resulted in further CI reduction of 4 % units. The small CI reduction suggests that when the CNFs are small enough, the effects of mechanical nanofibrillation on cellulose crystallinity become moderate (Hoeger et al. 2013).

SEM images (Fig. 3c, d) reveal that alg-CNF-10 and alg-CNF-20 achieve nano-scale in diameter with very high aspect ratios. The diameter distributions of both of the algal CNFs were mainly in the range of 10–40 nm with a peak between 20 and 25 nm (Fig. 4a, b). For alg-CNF-10, approximately 22.5 % of the fibrils had a diameter of 20–25 nm, while for alg-CNF-20, the number was approximately 32.5 %, and the distribution became narrower, suggesting increasing microfluidization produce CNFs with more uniform diameter.

CNF production from enzymatically pretreated BEP and algal cellulose

Mechanical nanofibrillation combined with enzymatic hydrolysis pretreatment has been proven to be an effective method to produce CNFs (Paakko et al. 2007; Wang et al. 2015). The effects of enzymatic hydrolysis on algal CNF productions were evaluated and compared with CNFs from enzymatically treated BEP. The enzymatically pretreated BEP and algal cellulose were fibrillated in the microfluidizer after 20 passes through a 200 μm chamber and additional 20 passes through an 87 μm chamber. The resulting CNFs were labeled as alg-CNF-enzy and BEP-CNF-enzy, respectively.

The extent of enzymatic treatment can be seen from the enzymatic hydrolysis solids yield. Under cellulose enzyme dosage of 3 FPU/g glucan, the solids yield of algal cellulose was higher than that of BEP for all the samples periodically collected as shown in Fig. 5. For both BEP and algal cellulose, initial solids hydrolysis was rapid as can be seen from the rapid solids yield reduction in the first 10 h. Enzymatic hydrolysis is a two-phase biochemistry process between cellulase and cellulose, and thus the greater the contact between the cellulases and the substrates, the higher the enzymatic hydrolysis efficiency (Leu and Zhu 2013). In early stage of enzymatic hydrolysis, the cellulase in the system had relatively high concentration and more chance to contact with cellulose resulting in rapidly decreased solids yield. After 48 h of enzymatic hydrolysis, the solids yields of BEP and algal cellulose were about 63 and 82 %, respectively. Looking at the wood pulp, one may see the BEP has a Segal CI of about 55 % (Qing et al. 2013). The algal cellulose is much more crystallized than BEP (Fig. 2) and thus is more difficult to hydrolyze (Zhao et al. 2007), resulting in a higher solids yield than that of BEP.

The Segal CI of algal CNFs and BEP CNFs produced from enzymatic pretreatment and microfluidization are shown in Fig. 2b, respectively. The BEP-CNF-enzy showed about 5 % units and the alg-CNF-enzy showed 12 % units decrease in CI,

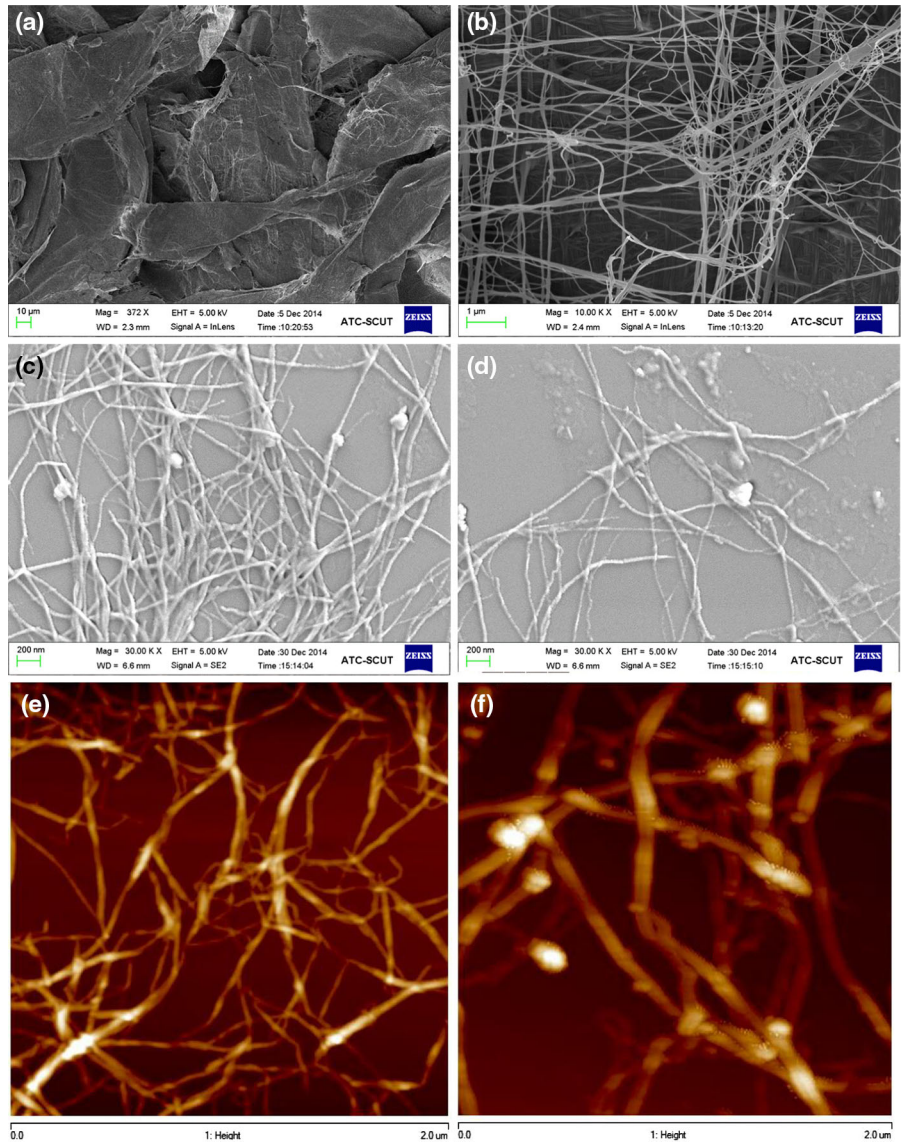

Fig. 3 SEM pictures of **a** algal cellulose at ×372, **b** algal cellulose at ×10,000, **c** alg-CNF-10 at ×30,000, and **d** alg-CNF-20 at ×30,000; AFM pictures of **e** alg-CNF-enzy and **f** BEP-CNF-enzy

compared to their original fibers. Although during BEP enzymatic treatment, crystallinity was increased due to the saccharification of amorphous cellulose (Zhu et al. 2011), the subsequent mechanical treatments would reduce BEP crystallinity (Wang et al. 2012; Hoeger et al. 2013). Following this reasoning one may explain that the BEP-CNF-enzy had decreased CI compared to untreated BEP. Algal cellulose has almost no amorphous region, but it has a higher specific surface area (Hua et al. 2014; Mihranyan 2011; Strømme et al. 2002) than BEP fibers. Therefore, enzyme directly attacks the crystallized cellulose though at a slow rate. As a result, algal CNFs produced by enzymatic hydrolysis plus microfluidization (alg-CNF-enzy) had a lower CI than the material produced by microfluidization only (alg-CNF-20; Fig. 2). The decreased crystallinity may allow efficient chemical modifications on algal CNFs for alternate properties and applications.

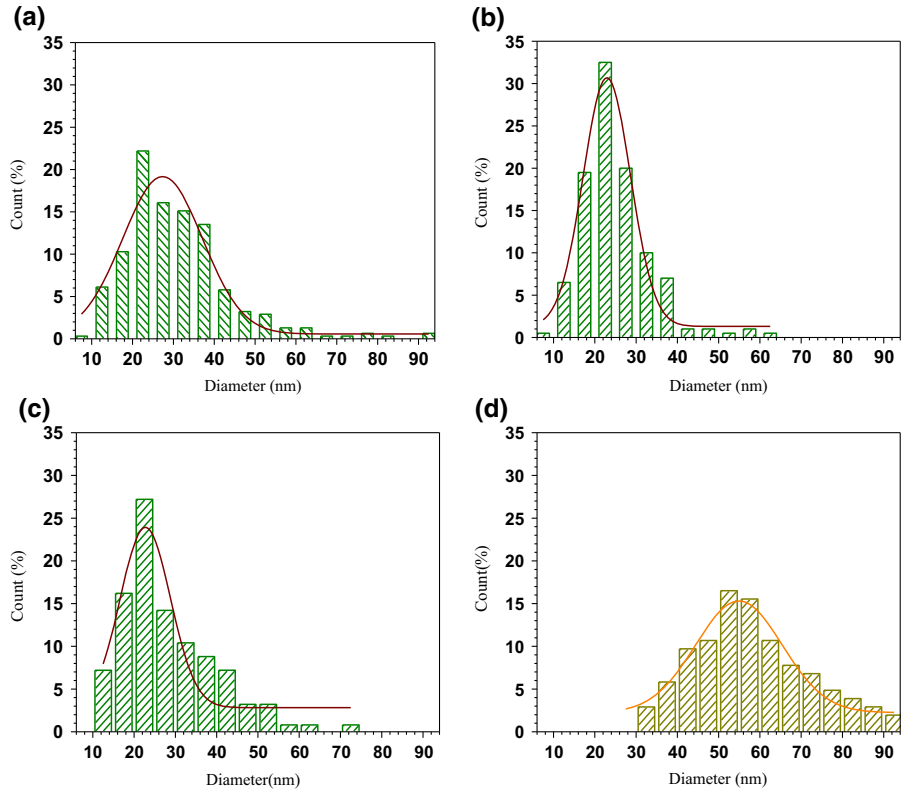

Fig. 4 Diameter distributions of **a** alg-CNF-10, **b** alg-CNF-20, **c** alg-CNF-enzy, and **d** BEP-CNF-enzy

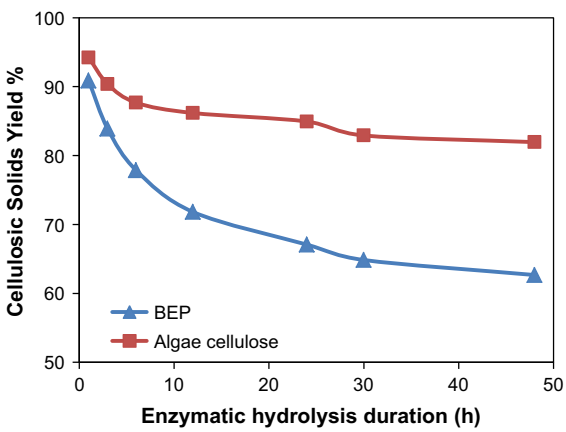

Fig. 5 Cellulosic solid yields after enzymatic hydrolysis of algal cellulose and BEP

From the AFM pictures (Fig. 3e, f), it can be seen that alg-CNF-enzy is smaller than BEP-CNF-enzy. From the diameter distribution analyses (Fig. 4c, d), the diameter of alg-CNF-enzy is mainly between 10 and 40 nm, while BEP-CNF-enzy is between 40 and 80 nm, more than two times larger than that of alg-CNF-enzy. The reason could be that the algal cellulose elementary microfibrils have a diameter of about 10 and 30 nm (Mihranyan 2011), 2–6 time larger than that of wood, and the microfibrils do not aggregate together but instead form a web-like structure (Fig. 3b). Consequently it may be easier to separate CNFs from algal cellulose than woody cellulose. By comparing algal CNFs produced by enzymatic hydrolysis and microfluidization (alg-CNF-enzy) and algal CNFs produced by microfluidization only (alg-CNF-20), the enzymatic hydrolysis does not have evident effects on the diameter distribution of algal CNFs. The alg-CNF-20 had most of its diameter between 10 and 40 nm (Fig. 4b), so it is very likely that microfluidization only is already able to separate the algal cellulose into its elementary microfibrils (10–30 nm), and enzymatic hydrolysis does not help to further separate the elementary microfibrils but instead decreased its crystallinity to a small extent.

Thermal properties were also investigated. BEP-CNF-enzy has four weight-loss peaks from the DTG curve (Fig. 6). The small peaks before 100 °C and at

180 °C may be due to the free water and bound water evaporations, accounting for about 25 % weight loss. The peak at 240 °C was likely due to hemicelluloses decomposition (Yang et al. 2007). Temperature of 315–400 °C is mainly the range for cellulose decomposition (Yang et al. 2007). The major weigh loss of more than 50 % with a peak at 326 °C should be due to cellulose decomposition. Different from BEP-CNF-enzy, alg-CNF-enzy only has one major weight loss peak at 390 °C, which is also very likely due to cellulose decomposition. The difference indicates that algal CNFs are highly crystalized having little bound water and has high purity without large content of hemicelluloses.

Crystal structures of CNFs produced from BEP and algae

Cellulose I is the most abundant cellulose polymorph in nature, which can also be classified into two polymorphs Iα and Iβ. Cellulose Iβ is dominant in higher plants including wood cellulose, while algal cellulose is composed of both polymorphs with a larger fraction of Iα (Koyama et al. 1997; Imai and Sugiyama 1998). The crystal information files of cellulose Iα and Iβ were obtained from previous studies by Nishiyama et al. (2002, 2003). The parameters of the Iα unit cell were a = 6.717 Å, b = 5.962 Å, c = 10.40 Å, α = 118.08°, β = 114.80°, and γ = 80.37°; the Iβ unit cell has a = 7.784 Å, b = 8.201 Å, c = 10.38 Å, α = 90.00°, β = 90.00°, and γ = 96.55°. The powder diffraction patterns as well as the dominant Miller Indices simulated by Mercury 3.0 of cellulose Iα and Iβ with random orientation are shown in Fig. 7.

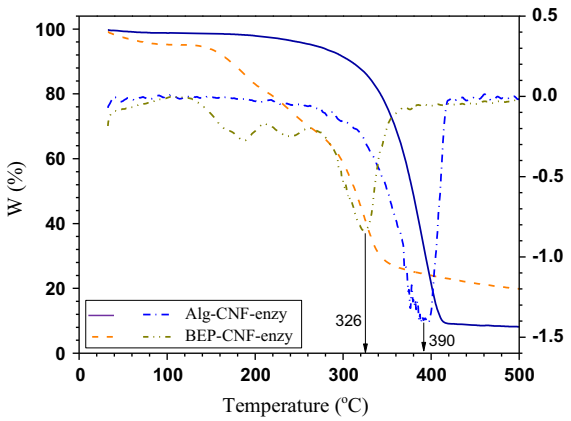

Fig. 6 TGA and DTG curves of algal CNFs and BEP CNFs produced by enzymatic hydrolysis and microfluidization

The experimental XRD spectra of the algal and BEP CNFs produced by enzymatic hydrolysis and microfluidization are shown in Fig. 8, which were dissimilar to the cellulose Iα and Iβ diffraction patterns shown in Fig. 7. The BEP CNF XRD spectrum can be simulated by adjusting the FWHM of cellulose Iβ diffraction pattern to 2.5° (Fig. 8a). Additionally, to the simulation, the parameters a = 7.73 Å, b = 7.70 Å and γ = 95.0° were used in order to better simulate the less-perfectly ordered BEP cellulose. Due to a large FWHM, peaks [1-10] and [110] overlap with each other and appear as a single broad peak (French and Santiago Cintrón 2013).

The algal CNF XRD spectrum (Fig. 8b) was simulated based on a standard cellulose Iα diffraction pattern by using a FWHM of 0.8°. The β parameter was adjusted to 116.0° in order to better simulate the less-perfectly ordered algal cellulose. The experimental spectrum also indicates the algal CNFs have a preferred orientation along the [100] axis and the [010] axis. However, Mercury 3.0 software can only simulate preferred orientation along one axis. Consequently, we are assuming the algal CNFs are a hybrid of cellulose Iα with preferred orientation along the [100] axis and cellulose Iα with preferred orientation along the [010] axis. Therefore the cellulose Iα hybrid diffraction patterns can be simulated as:

$$\text{Intensity}_{\text{Hybrid}} = \text{Intensity}_{100} \times P_{100} + \text{Intensity}_{010} \times (1 - P_{100})$$

where P_{100} is the percentage of cellulose Iα with preferred orientation along the [100] axis. The March–Dollase factor for both preferred orientation ([100] and [010]) was set to 0.65. By adjusting the P_{100} value, we found that when P_{100} equals 75 %, the simulated algal CNF XRD pattern agrees very well with the experimental pattern (Fig. 8b). The simulation can be interpreted as that 75 % of the algal CNF sample has a fraction of crystallites (March–Dollase factor = 0.65) having preferred orientation along [100] axis; while 25 % of the algal CNF sample has a fraction of crystallites (March–Dollase factor = 0.65) having preferred orientation along [010] axis (Fig. 9). Algal CNFs have more preferred orientations than pulp CNFs could possibly be explained by the web-like structure of algal microfibrils (Fig. 3b). Some large microfibril bundles from algal CNF samples may

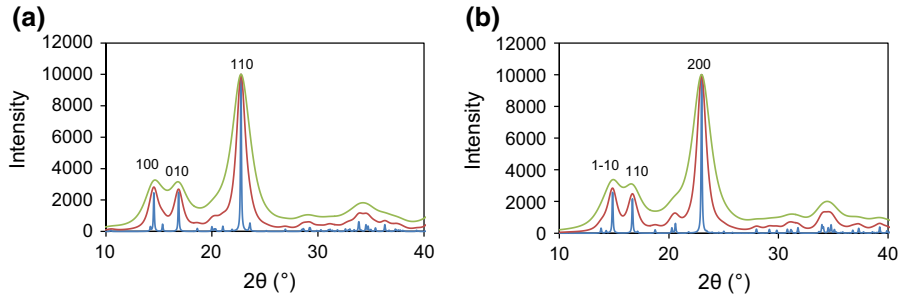

Fig. 7 Simulated diffraction patterns of **a** cellulose Iα and **b** cellulose Iβ (from *outer* to *inner graph*, FWHM is 2.0, 1.0 and 0.1° respectively)

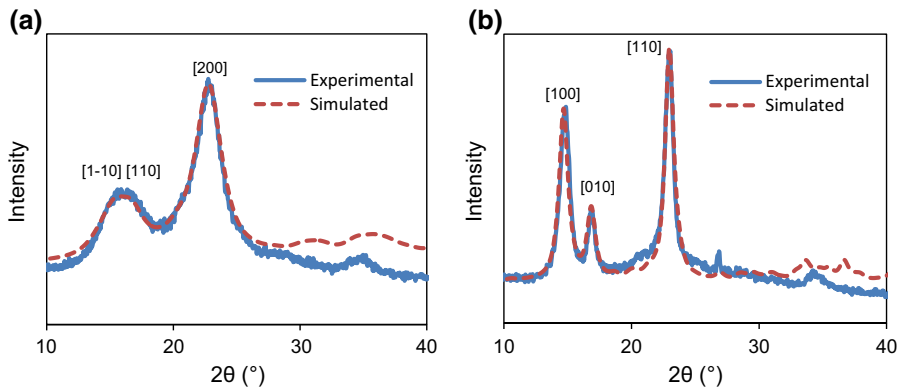

Fig. 8 XRD spectra of **a** BEP and **b** algal CNFs from experiment and simulation (simulation of BEP CNF: cellulose Iβ with random orientation, FWHM = 2.5°, **a** 7.73 Å, **b** 7.70 Å and γ = 95.0°; Simulation of algal CNF: FWHM = 0.8°, β = 116.0°, 75 % cellulose Iα with preferred orientation along the [100] axis, 25 % along the [010] axis, and March–Dollase factor = 0.65)

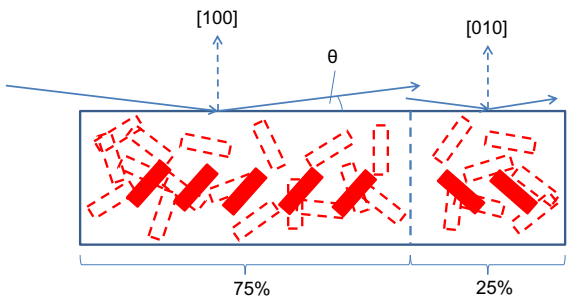

Fig. 9 Drawing showing the hybrid of algal CNFs. The hybrid can be interpreted as 75 % of the algal CNF sample has a fraction of cellulose Iα crystallites (March–Dollase factor = 0.65) having preferred orientation along the [100] axis; while 25 % of it has a fraction of crystallites (March–Dollase factor = 0.65) having preferred orientation along the [010] axis

still contain several microfibrils, which likely has preferred orientations along the [100] or [010] axes due to the microfibrils intertwining with each other.

Additionally, the smaller FWHM of algal CNFs than BEP CNFs may also agree with its larger Segal CI (French and Santiago Cintrón 2013). The crystallite widths of BEP and algal CNFs were calculated as 3.6 and 11.3 nm (Table 1), respectively, which are consistent with their elementary microfibril widths of ~5 and 10–30 nm (Mihranyan 2011). The crystallite lengths of BEP and algal CNFs were calculated as 37.0 and 118.7 nm (Table 1), respectively. The calculated crystallite width and length of the BEP CNFs were also comparable to CNFs produced from other types of pulps (Leppänen et al. 2009).

Table 1 Crystallite sizes of algal and BEP CNFs

CNF source	FWHM (°)	Crystallite width (nm)	Crystallite length (nm)
C. glomerata	0.8	11.3	118.7
BEP	2.5	3.6	37.0

Conclusions

Cellulose was extracted from algae *Cladophora glomerata* and processed into cellulose nanofibrils (CNFs). Increasing microfluidization times produced CNFs with smaller and more uniform size (diameter) and lower crystallinity. However, enzymatic pretreatment had very limited effects on algal CNF diameter, likely due to the diameter of algal CNFs produced by only microfluidization having already reached the microfibril levels. Nevertheless, enzymatic pretreatment could decrease algal CNFs' crystallinity by a small amount. Even though algal cellulose had a very high crystallinity, it is likely that enzyme was still able to degrade the crystallized algal cellulose due to its high specific surface area. CNFs produced from bleached eucalyptus pulp (BEP) had much lower crystallinity, larger diameter and worse thermal stability than algal CNFs produced by the same methods, indicating algal CNFs to be a novel and promising nano-materials.

The simulation of XRD patterns of algal and BEP CNFs suggested that: (1) the cellulose Iβ crystallites in BEP CNFs probably have a random orientation. (2) The algal CNFs are likely a hybrid of cellulose Iα crystallites with a fraction of 75 % having a preferred orientation along the [100] axis and another 25 % having a preferred orientation along the [010] axis; the March–Dollase factor for both preferred orientations was 0.65.

Acknowledgments This work was supported by the National Natural Science Foundation of China (31400512) and US Department of Agriculture NIFA, under Critical Agricultural Material Grant (2013-38202-20400). The authors would like to give their appreciations to Dr. Alfred French for personal communications about the simulation of XRD patterns and to Dr. Renil Anthony for his assistance with algae collection.

References

Alemdar A, Sain M (2008) Isolation and characterization of nanofibers from agricultural residues—wheat straw and soy hulls. Bioresour Technol 99:1664–1671

Auer MT, Tomlinson LM, Higgins SN, Malkin SY, Howell ET, Bootsma HA (2010) Great Lakes Cladophora in the 21st century: same algae-different ecosystem. J Great Lakes Res 36:248–255

Camacho DH, Gerongay SRC, Macalinao JPC (2013) *Cladophora* cellulose-polyaniline composite for remediation of toxic chromium (VI). Cell Chem Technol 47:125–132

French AD (2014) Idealized powder diffraction patterns for cellulose polymorphs. Cellulose 21:885–896

French AD, Santiago Cintrón M (2013) Cellulose polymorphy, crystallite size, and the segal crystallinity index. Cellulose 20:583–588

Henriksson M, Henriksson G, Berglund LA, Lindstrom T (2007) An environmentally friendly method for enzyme-assisted preparation of microfibrillated cellulose (MFC) nanofibers. Eur Polym J 43:3434–3441

Hoeger IC, Nair SS, Ragauskas AJ, Deng Y, Rojas OJ, Zhu JY (2013) Mechanical deconstruction of lignocellulose cell walls and their enzymatic saccharification. Cellulose 20:807–818

Hua K, Carlsson DO, Alander E, Lindstrom T, Stromme M, Mihranyan A, Ferraz N (2014) Translational study between structure and biological response of nanocellulose from wood and green algae. RSC Adv 4:2892–2903

Hult EL, Larsson PT, Iversen T (2001) Cellulose fibril aggregation—an inherent property of kraft pulps. Polymer 42:3309–3314

Imai T, Sugiyama J (1998) Nanodomains of Iα and Iβ cellulose in algal microfibrils. Macromolecules 31:6275–6279

Iwamoto S, Nakagaito AN, Yano H (2007) Nano-fibrillation of pulp fibers for the processing of transparent nanocomposites. Appl Phys A Mater 89:461–466

Jagadeesh D, Reddy DJP, Rajulu AV (2011) Preparation and properties of biodegradable films from wheat protein isolate. J Polym Environ 19:248–253

Koyama M, Sugiyama J, Itoh T (1997) Systematic survey on crystalline features of algal celluloses. Cellulose 4:147–160

Leppänen K, Andersson S, Torkkeli M, Knaapila M, Kotelnikova N, Serimaa R (2009) Structure of cellulose and microcrystalline cellulose from various wood species, cotton and flax studied by X-ray scattering. Cellulose 16:999–1015

Leu SY, Zhu JY (2013) Substrate-related factors affecting enzymatic saccharification of lignocelluloses: our recent understanding. Bioenerg Res 6:405–415

Macrae CF, Gruno IJ, Chisholm JA, Edgington PR, McCabe P, Pidcock E, Rodriguez-Monge L, Taylor R, van de Streek J, Wood PA (2008) Mercury CSD 2.0-new features for the visualization and investigation of crystal structures. J Appl Crystallogr 41:466–470

Mihranyan A (2011) Cellulose from *Cladophorales* green algae: from environmental problem to high-tech composite materials. J Appl Polym Sci 119:2449–2460

Mihranyan A, Andersson SB, Ek R (2004) Sorption of nicotine to cellulose powders. Eur J Pharm Sci 22:279–286

Moon RJ, Martini A, Nairn J, Simonsen J, Youngblood J (2011) Cellulose nanomaterials review: structure, properties and nanocomposites. Chem Soc Rev 40:3941–3994

Moran JI, Alvarez VA, Cyras VP, Vazquez A (2008) Extraction of cellulose and preparation of nanocellulose from sisal fibers. Cellulose 15:149–159

Mwaikambo LY, Ansell MP (2002) Chemical modification of hemp, sisal, jute, and kapok fibers by alkalization. J Appl Polym Sci 84:2222–2234

Nelson ML, O'Connor RT (1964) Relation of certain infrared bands to cellulose crystallinity and crystal lattice type. Part II. A new infrared ratio for estimation of crystallinity in celluloses I and II. J Appl Polym Sci 8:1325–1341

Nishiyama Y, Langan P, Chanzy H (2002) Crystal structure and hydrogen-bonding system in cellulose Iβ from synchrotron X-ray and neutron fiber diffraction. J Am Chem Soc 124:9074–9082

Nishiyama Y, Sugiyama J, Chanzy H, Langan P (2003) Crystal structure and hydrogen bonding system in cellulose Iα, from synchrotron X-ray and neutron fiber diffraction. J Am Chem Soc 125:14300–14306

Paakko M, Ankerfors M, Kosonen H, Nykanen A, Ahola S, Osterberg M, Ruokolainen J, Laine J, Larsson PT, Ikkala O, Lindstrom T (2007) Enzymatic hydrolysis combined with mechanical shearing and high-pressure homogenization for nanoscale cellulose fibrils and strong gels. Biomacromolecules 8:1934–1941

Qing Y, Sabo R, Zhu JY, Agarwal U, Cai Z, Wu Y (2013) A comparative study of cellulose nanofibrils disintegrated via multiple processing approaches. Carbohyd Polym 97:226–234

Reddy N, Yang Y (2005) Biofibers from agricultural byproducts for industrial applications. Trends Biotechnol 23:22–27

Segal L, Creely JJ, Martin AE, Conrad CM (1959) An empirical method for estimating the degree of crystallinity of native cellulose using the X-ray diffractometer. Text Res J 29: 786–794

Siro I, Plackett D (2010) Microfibrillated cellulose and new nanocomposite materials: a review. Cellulose 17:459–494

Spence KL, Venditti RA, Rojas OJ, Habibi Y, Pawlak JJ (2011) A comparative study of energy consumption and physical properties of microfibrillated cellulose produced by different processing methods. Cellulose 18:1097–1111

Strømme M, Mihranyan A, Ek R (2002) What to do with all these algae? Mater Lett 57:569–572

Wang Q, Zhu JY (2015) Facile preparation of nanofiller-paper using mixed office paper without deinking. Tappi J 14:167–174

Wang QQ, Zhu JY, Gleisner R, Kuster TA, Baxa U, McNeil SE (2012) Morphological development of cellulose fibrils of a bleached eucalyptus pulp by mechanical fibrillation. Cellulose 19:1631–1643

Wang W, Mozuch MD, Sabo RC, Kersten P, Zhu JY, Jin Y (2015) Production of cellulose nanofibrils from bleached eucalyptus fibers by hyperthermophilic endoglucanase treatment and subsequent microfluidization. Cellulose 22:351–361

Yang H, Yan R, Chen H, Lee DH, Zheng C (2007) Characteristics of hemicellulose, cellulose and lignin pyrolysis. Fuel 86:1781–1788

Yue Y, Han J, Han G, Zhao Q, French AD, Wu Q (2015) Characterization of cellulose I/II hybrid fibers isolated from energycane bagasse during the delignification process: morphology, crystallinity and percentage estimation. Carbohyd Polym 133:438–447

Zhao H, Kwak JH, Zhang ZC, Brown HM, Arey BW, Holladay JE (2007) Studying cellulose fiber structure by SEM, XRD, NMR and acid hydrolysis. Carbohyd Polym 68:235–241

Zhu JY, Sabo R, Luo X (2011) Integrated production of nanofibrillated cellulose and cellulosic biofuel (ethanol) by enzymatic fractionation of wood fibers. Green Chem 13:1339–1344